Advances in Nano Research, *Vol. 16, No. 4 (2024) 325-340*
https://doi.org/10.12989/anr.2024.16.4.325

Comparative analysis on darcy-forchheimer flow of 3-D MHD hybrid nanofluid (MoS_2−Fe_3O_4/H_2O) incorporating melting heat and mass transfer over a rotating disk with dufour and soret effects

A.M. Abd-Alla[1a], Esraa N. Thabet[*2], S.M.M.El-Kabeir[2b], H. A. Hosham[3c] and Shimaa E. Waheed[4d]

[1]*Department of Mathematics*, *Faculty of Science*, *Sohag University*, *Sohag*, *Egypt*
[2]*Department of Mathematics*, *Faculty of Science*, *Aswan University*, *Aswan 81528 Egypt*
[3]*Department of Mathematics*, *Faculty of Science*,*Taibah University*, *Yanbu 41911*, *Saudi Arabia*
[4]*Department of Mathematics*, *Faculty of Science*, *Benha University*, *Benha*, *Egypt*

(*Received April 30, 2023, Revised January 10, 2024, Accepted January 27, 2024*)

Abstract. There are several novel uses for dispersing many nanoparticles into a conventional fluid, including dynamic sealing, damping, heat dissipation, microfluidics, and more. Therefore, melting heat and mass transfer characteristics of a 3-D MHD Hybrid Nanofluid flow over a rotating disc with presenting dufour and soret effects are assessed numerically in this study. In this instance, we investigated both ferric sulfate and molybdenum disulfide as nanoparticles suspended within base fluid water. The governing partial differential equations are transformed into linked higher-order non-linear ordinary differential equations by the local similarity transformation. The collection of these deduced equations is then resolved using a Chebyshev spectral collocation-based algorithm built into the Mathematica software. To demonstrate how different instances of hybrid/ nanofluid are impacted by changes in temperature, velocity, and the distribution of nanoparticle concentration, examples of graphical and numerical data are given. For many values of the material parameters, the computational findings are shown. Simulations conducted for different physical parameters in the model show that adding hybrid nanoparticle to the fluid mixture increases heat transfer in comparison to simple nanofluids. It has been identified that hybrid nanoparticles, as opposed to single-type nanoparticles, need to be taken into consideration to create an effective thermal system. Furthermore, porosity lowers the velocities of simple and hybrid nanofluids in both cases. Additionally, results show that the drag force from skin friction causes the nanoparticle fluid to travel more slowly than the hybrid nanoparticle fluid. The findings also demonstrate that suction factors like magnetic and porosity parameters, as well as nanoparticles, raise the skin friction coefficient. Furthermore, It indicates that the outcomes from different flow scenarios correlate and are in strong agreement with the findings from the published literature. Bar chart depictions are altered by changes in flow rates. Moreover, the results confirm doctors' views to prescribe hybrid nanoparticle and particle nanoparticle contents for achalasia patients and also those who suffer from esophageal stricture and tumors. The results of this study can also be applied to the energy generated by the melting disc surface, which has a variety of industrial uses. These include, but are not limited to, the preparation of semiconductor materials, the solidification of magma, the melting of permafrost, and the refreezing of frozen land.

Keywords: Chebyshev spectral collocation technique; dufour and soret effects; hybrid nanofluid; joule heating; melting heat and mass transfer; rotating disk; viscous dissipation

1. Introduction

Throughout the past two decades, engineers and scientists have developed an interest in nanofluid flow. Nanofluid is a cutting-edge engineering material with several uses in the sectors of heat exchangers, biology, nuclear industries, Oil and drilling recovery, cancer detection, electronic cooling, vehicle cooling, vehicle heat management, and cooling of microelectronics. Utilizing (ZnO) nanoparticles, (Ajeel *et al*. 2019) numerically examined the effectiveness of the thermal behavior of semi-circles, houses-shaped channels, and trapezoids. While taking into account the impacts of thermal radiation and heat absorption, (Renuka *et al*. 2020) reported the phenomena of entropy formation in nanofluid flow among two stretchable rotating discs and discovered that it reduced with increasing temperature ratio. The thermal effect caused by cross nanofluid involving applications of the bio-convection phenomena was communicated by (Aljaloud *et al*. 2023). It was appropriate to include the additional thermal effect of the radiated phenomenon, viscous dissipation, and activation energy. The findings showed how the interplay of the first-order slip parameter decreased the velocity profile. Hybrid nanofluids are a brand-new modern and cutting-edge type of nanofluid. More investigation into nanofluid models is being performed (Benmansour *et al*. 2019, Letti *et al*. 2017, Rezaee *et al*. 2022, Sharif *et al*. 2021a, b, Wang *et al*. 2021, Yanzhen *et al*. 2021). To create hybrid nanofluids, two different types

*Corresponding author, Ph.D.,
E-mail: mesraa422@gmail.com
[a] Professor., E-mail: mohmrr@yahoo.com
[b] Professor, E-mail: elkabeir@yahoo.com
[c] Professor, E-mail: hanyalbadrey@yahoo.com
[d] Professor, E-mail: shimaa_ezat@yahoo.com

ISSN: 2287-237X (Print), 2287-2388 (Online)

of nanoparticles are suspended in a fluid. This makes it possible for the unique thermophysical characteristics of the various nanoparticles to interact with one another in beneficial ways. To strengthen the thermal impacts of various flow dynamics, a hybrid nanofluidic system is being developed and evaluated. Hybrid nanofluids offer uses across a broad spectrum in the manufacturing of medical items, transfer cooling, heating systems, solar panels, and electronic chips, among other industries (Babar and Ali 2019). Current research studies and investigations have looked at how hybrid nanofluids can transport heat more efficiently than conventional single-particle nano-fluids (Khan *et al*. 2023, Mahanthesh *et al*. 2019, Reddy *et al*. 2021, Shoaib *et al*. 2021). For the manufacture of nanofluids and hybrid nanofluids, a range of nanoparticles is available. Every type of material has a unique set of benefits and drawbacks depending on each material's specific features. The "Aluminum nanoparticle" has various advantages over other well-known nanomaterials in the industrial and technical domains, claim (Farhana *et al*. 2019). Le *et al*. (2024) used graphene oxide with molybdenum disulfide nanoparticles via an inclined plate to construct a fractional hybrid nanofluid model. The thermal characteristic of the hybrid nanofluid model when mixed convection and magnetic force are present is taken into account. The Laplace transform approach was used to solve this model. Furthermore, the explanation of (Yasinskiy *et al*. 2018) shows how the thermophysical parameters for the nanofluid containing (TiO_2) nanoparticles were calculated from the thermal conductivity. By employing a molecular dynamics (MD) simulation, (Banawas *et al*. 2023) investigated the effects of adding zinc ion nanoparticles on the mechanical and thermal properties of calcium phosphate cement (CPC).

Several scholars have looked at the hydrodynamic movement of a viscous, incompressible fluid in a rotating space. While considering various parts of the topic due to the problems with the liquefied flow in a rotating medium. Because of their importance to geophysics, astrophysics, and hydraulic engineering, as well as their use, the issues of hydromagnetic flow in a rotating environment have attracted a lot of attention in recent years. The stabilization and long-term changes in the earth's magnetic field caused by motion in its molten core, the structure of rotating magnetic stars, the rate at which the sun rotates internally, problems with planetary and solar dynamos, turbomachines, revolving drum-type separators and rotating hydromagnetic generators operate in a closed-loop, two-phase MHD generator flow, and other significant issues are just a few of the many important ones. Given all of its applications in engineering and industry, attention has recently turned to the examination of fluid flow in rotating discs. In the MHD nanofluid flows by a rotating disc, (Imtiaz *et al*. 2019) addressed melting heat transport. For, references (Rashid *et al*. 2023, Vijay and Sharma 2023), some insightful study findings in this field are given.

The radiation effect has opened up several opportunities in the fields of physics and a variety of sectors, such as glass manufacturing, polymer processing, nuclear reactors, and space technologies, including power plants and rockets. When a magnetic field is present, Reddy and Goud (Reddy and Shankar Goud 2023) investigated how changes in temperature gradient affected the flow of a water-based nanofluid passing through an infinite flat disc exhibiting radiative heat transfer. Several scholars examined the different fluid flow through various surfaces to take into account the Arrhenius activation energy, melting heat transfer, as well as Soret and Dufour impacts (Islam *et al*. 2023, Patil *et al*. 2023, Khan *et al*. 2022).

Motivated by the scientific literature cited above, where numerous researchers looked into and analyzed various kinds of nanofluids and hybrid nanofluids to see their fascinating thermal qualities. A significant amount of research has been conducted using multiple mathematical models (Vanaki *et al*. 2016, Lv *et al*. 2021, Bayones *et al*. 2022, Bhatti and Abdelsalam 2021) with varied physical implementations, but only a small number of these studies used contemporary numerical approaches to address the complex issues with hybrid nanofluids. This research aims to analyze the Darcy-Forchheimer flow in a 3-D MHD hybrid nanofluid over a rotating disc underneath the influences of melting heat and mass transfer, magnetic field, thermal radiation, and cross-diffusion (Dufour and Soret effects) by using the Chebyshev spectral collocation approach (Deville 1990, El-gendi 1969, Ellahi *et al*. 2014, Le *et al*. 2023, Parand *et al*. 2017). To meet our needs, requisite tables and graphs are developed. Additionally, comparisons between hybrid and regular nanofluid have been demonstrated. Even though nanofluids meet engineers' demands for the best possible thermal performance, a fluid with strong thermal conductivity is still necessary. Because of this, a better nanocomposite fluid "hybrid nanofluids" with higher heat conductivity than nanofluids has been established. Therefore, the author's ultimate goal is to disclose the technologically level feature of hybrid nanosuspension. These are the key features of this study:

- The investigation water-based base fluid containing nanoparticles of ferric sulfate and molybdenum disulfide.
- Melting heat and mass flow have been predicted in a unique numerical approach for 3-D hybrid nanofluid-based laminar constant MHD Darcy-Forchheimer flow over a rotating disc. By adopting an appropriate similarity transformation, the governing equations with the help of (PDEs) are then condensed into a non-linear coupled system of (ODEs). As a result, the equations have mapped onto the finite domain region, allowing us to extract derivatives of various orders.
- It takes innovative work to fully implement the Chebyshev spectral collocation approach using Mathematica software to obtain the necessary solution to such a dilemma.
- With the numerical analysis of flow problems, it has been possible to learn more about how velocity, temperature, and concentration fields fluctuate as well as how skin friction, Nusselt, and Sherwood numbers behave in response to different physical constraints.

The work's innovative results are important in a variety of scientific and industrial fields including power generation, heat exchangers, thermal systems, aircraft, rotating turbomachinery, automobiles, materials, renewable energy sources, chemical processing, and industrial

equipment (AlDosari *et al*. 2023, Henda *et al*. 2023, Le, *et al*. 2023, Li and Tlili 2023, Tlili *et al*. 2023). They also help determine how well hybrid nanoparticles perform in non-Newtonian fluids. The findings of this study have the potential to significantly improve thermal energy system competence and efficiency in several industrial, engineering, and biological fields in an economical and environmentally responsible manner. To the best of our knowledge, there are relatively few published works on hybrid nanofluid problems, and no research that addresses the topics included in this article has been published. Our endeavor is therefore both original and distinct. The mathematical explanation of our model will now be explained in the following sections, which will be followed by necessary discussions.

2. Mathematical configuration

2.1 Geometric structure

Consider we have an incompressible hybrid nanofluid that exhibits radiation, Soret, and Dufours effects while flowing laminar in three dimensions around a rotating disc surrounded by a porous medium. In fields where the high flow rate impact frequently occurs, such as petroleum engineering, the Darcy-Forchheimer flow effect is essential. Additionally, some activities, including heat transport and geophysical design, require porous media. Numerous other devices, including solar receivers and energy storage systems, are also impacted. It is presumed that the disc revolves with constant angular velocity Ω and is positioned at $z = 0$, that z is considered to be the vertical axis in the cylindrical coordinates system (r, Φ, z). The disc is assumed to rotate at a constant angular velocity Ω, and to be located at $z = 0$. In the cylindrical coordinate system (r, Φ, z), z represents the vertical axis. The $(r\Phi)$ plane is used to organize the surface. When melting occurs in the steady-state porous matrix, a rotating disc acts as the interface between the solid and liquid phases. At a temperature T_m that is steady throughout the disc, the porous matrix's substance melts. Temperatures of the solid far from the interface T_0 $(T_0 < T_m)$, and the liquid layer T_∞ $(T_\infty > T_m)$. The nanoparticles' electrical conductivity is also a result of the magnetic force's applied properties. In addition to improving the thermal efficiency of heat exchangers, this present research may also be useful in maintaining thermal balance management in small heat-density equipment and gadgets. The model is prepared based on the subsequent assumptions:

• Rheology of "MoS_2−Fe_3O_4/H_2O" hybrid nanofluid is examined.

• The flow has a three-dimensional cylinder system and is steady and incompressible.

• With an angle of Ω, the disc rotates around the z − axis.

• The accessories of several prominent flow and thermal field limitations are examined such as thermal radiation as well as Dufour and Soret Effects.

• The influences of porous media and Darcy-Forchheimer

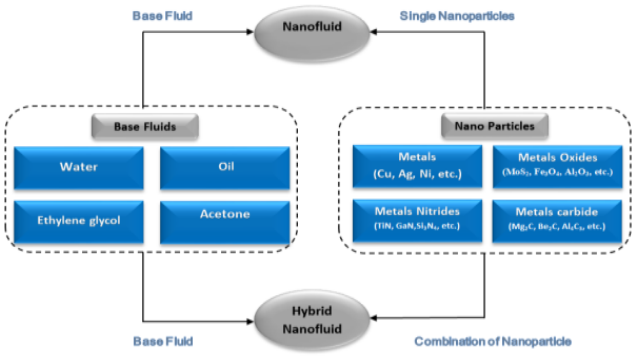

(a) Built-up process for hybrid nanofluids and nanofluids

(b) Nanoparticle size and geometrical appearance

Fig. 1 Hybrid nanofluids and nanofluids

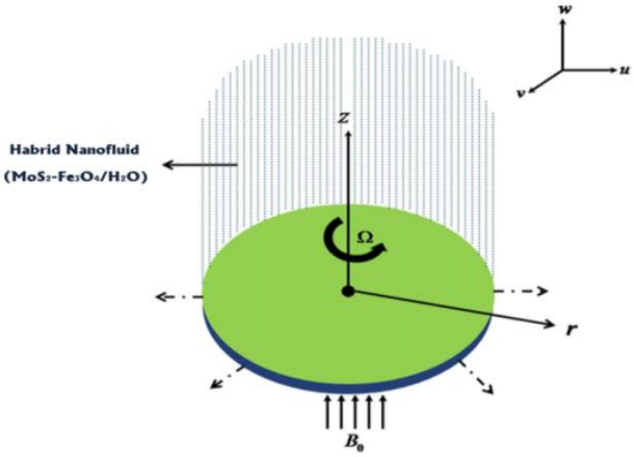

Fig. 2 Illustration of the geometric flow model

are specified.

• Thermal properties of nanoparticles are comprised.

• (Fig. 1) depicts the manufacturing scheme for both conventional and hybrid nanofluids as well as their size.

• (Fig. 2) displays the flow model and coordinate scheme.

(Fig. 3) portrays the flow diagram of the mathematical model.

2.2 Model description

This study investigates how hybrid nanoparticles affect the flow over a spinning disc when varying external effects are present. In this case, we considered molybdenum disulfide and ferrous sulfate to be nanoparticles suspended in water. The use of molybdenum disulfide nanoparticles in

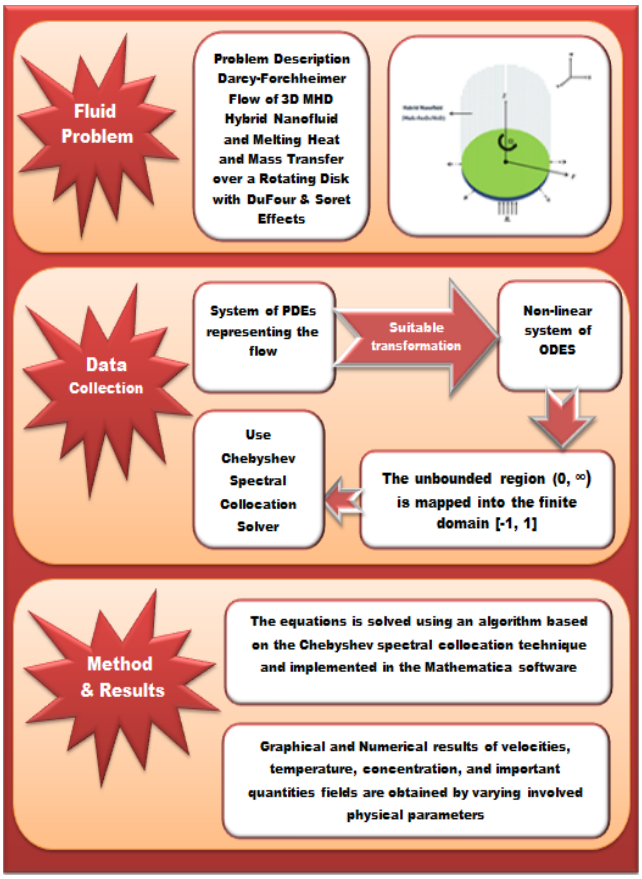

Fig. 3 Employed flow chart

biology, electronics, catalysis, and energy production is widespread. They are also anticipated to become more prominent as agents for environmental uses. It has been shown that molybdenum disulfide nanoparticles enhance plants' microbial capabilities. Additionally, they exhibit distinct catalytic and electronic behavior and may be used as a refining agent in the crude oil processing business as well as in the chemical synthesis of various materials. Apart from that, the most popular supplement for managing anemia is ferrous sulfate. Table 1 presents the qualities of their thermophysical properties along with the base fluid.

2.3 Governing equations

According to the standard boundary-layer and Boussinesq estimations, the mathematical equations for momentum, energy, and diffusion that characterize the flow model can be written as

(Mahanthesh *et al*. 2019, Eddy *et al*. 2021, Shoaib *et al*. 2021):

$$\frac{\partial u}{\partial r}+\frac{u}{r}+\frac{\partial w}{\partial z}=0, \tag{1}$$

$$u\frac{\partial u}{\partial r}-\frac{v^2}{r}+w\frac{\partial u}{\partial z}=\nu_{hnf}\left(\frac{\partial^2 u}{\partial r^2}+\frac{1}{r}\frac{\partial u}{\partial r}-\frac{u}{r^2}+\frac{\partial^2 u}{\partial z^2}\right) -\nu_{hnf}\frac{u}{k_1}-Fu^2-\frac{\sigma_{hnf}}{\mu_{hnf}}B_0^2 u, \tag{2}$$

$$u\frac{\partial v}{\partial r}+\frac{uv}{r}+w\frac{\partial v}{\partial z}=\nu_{hnf}\left(\frac{\partial^2 v}{\partial r^2}+\frac{1}{r}\frac{\partial v}{\partial r}-\frac{v}{r^2}+\frac{\partial^2 v}{\partial z^2}\right) -\nu_{hnf}\frac{v}{k_1}-Fv^2-\frac{\sigma_{hnf}}{\mu_{hnf}}B_0^2 v, \tag{3}$$

$$u\frac{\partial T}{\partial r}+w\frac{\partial T}{\partial z} =\left(\alpha_{hnf}+\frac{16}{3}\frac{\sigma^* T_\infty^3}{k^*\left(\rho c_p\right)_{hnf}}\right)\left[\frac{\partial^2 T}{\partial r^2}+\frac{1}{r}\frac{\partial T}{\partial r}+\frac{\partial^2 T}{\partial z^2}\right] +\frac{\sigma_{hnf}}{\left(\rho c_p\right)_{hnf}}B_0^2(u^2+v^2)+\frac{D_{hnf}K_{hnf}}{Cs_1\left(c_p\right)_{hnf}}\left(\frac{\partial^2 C}{\partial r^2}+\frac{1}{r}\frac{\partial C}{\partial r}+\frac{\partial^2 C}{\partial z^2}\right) +\frac{\mu_{hnf}}{\left(\rho c_p\right)_{hnf}}\left(\left(\frac{\partial u}{\partial z}\right)^2+\left(\frac{\partial v}{\partial z}\right)^2\right)+\frac{Q}{\left(\rho c_p\right)_{hnf}}(T-T_\infty), \tag{4}$$

$$u\frac{\partial C}{\partial r}+w\frac{\partial C}{\partial z}=D_{hnf}\left(\frac{\partial^2 C}{\partial r^2}+\frac{1}{r}\frac{\partial C}{\partial r}+\frac{\partial^2 C}{\partial z^2}\right) +\frac{D_{hnf}K_{hnf}}{T_m}\left(\frac{\partial^2 T}{\partial r^2}+\frac{1}{r}\frac{\partial T}{\partial r}+\frac{\partial^2 T}{\partial z^2}\right). \tag{5}$$

The boundary conditions are the following:

$$u=0,\ v=r\Omega,\ w=0,\ T=T_m,\ C=C_m\ at\ z=0 \qquad u\to 0,\ v\to 0,\ T\to T_\infty,\ C\to C_\infty\ as\ z\to\infty \tag{6}$$

And

$$K_{hnf}\left(\frac{\partial T}{\partial z}\right)_{z=0}=\rho_{hnf}\left(\lambda_3+Cs_2(T_m-T_0)\right)w(r,0) \tag{7}$$

The boundary condition (Eq.7) explains the heat transferred to the melting surface is equal to the heat needed to rise the temperature of surface from T_0 to T_m (i.e., the melting temperature) plus heat of melting [see (Imtiaz *et al*. 2019)].

The different thermophysical properties of hybrid nanofluid have mathematical expressions (Reddy *et al*. 2021, Shoaib *et al*. 2021):

$$\begin{aligned}
\mu_{hnf} &= \frac{\mu_f}{[(1-\varphi_1)(1-\varphi_2)]^{\frac{1}{2}}},\\
D_{hnf} &= D_f\,[(1-\varphi_1)(1-\varphi_2)]^{\frac{1}{2}},\\
\rho_{hnf} &= \rho_f\left[\left(\frac{\rho_{s1}}{\rho_f}\right)\varphi_1+(1-\varphi_1)\right](1-\varphi_2)+\varphi_2\rho_{s2},\\
\left(\rho c_p\right)_{hnf} &= \left(\rho c_p\right)_f\left[\left(\frac{\left(\rho c_p\right)_{s1}}{\left(\rho c_p\right)_f}\right)\varphi_1+(1-\varphi_1)\right](1-\varphi_2)+\varphi_2\left(\rho c_p\right)_{s2},\\
\alpha_{hnf} &= \frac{K_{hnf}}{\left(\rho c_p\right)_{hnf}},\\
\frac{K_{hnf}}{K_{nf}} &= \frac{K_{s2}+K_{nf}(s-1)-\varphi_2\left(K_{nf}-K_{s2}\right)(s-1)}{\left(K_{nf}-K_{s2}\right)\varphi_2+K_{nf}(s-1)+K_{s2}},\\
\frac{K_{nf}}{K_f} &= \frac{K_{s1}+K_f(s-1)-\varphi_1\left(K_f-K_{s1}\right)(s-1)}{\left(K_f-K_{s1}\right)\varphi_1+K_f(s-1)+K_{s1}},\\
\frac{\sigma_{hnf}}{\sigma_{nf}} &= \frac{\sigma_{s2}+\sigma_{nf}(s-1)-\varphi_2\left(\sigma_{nf}-\sigma_{s2}\right)(s-1)}{\left(\sigma_{nf}-\sigma_{s2}\right)\varphi_2+\sigma_{nf}(s-1)+\sigma_{s2}},\\
\frac{\sigma_{nf}}{\sigma_f} &= \frac{\sigma_{s1}+\sigma_f(s-1)-\varphi_1\left(\sigma_f-\sigma_{s1}\right)(s-1)}{\left(\sigma_f-\sigma_{s1}\right)\varphi_1+\sigma_f(s-1)+\sigma_{s1}}.
\end{aligned} \tag{8}$$

For a similarity solution, we introduce the following dimensionless variables (Shoaib *et al*. 2021):

$$\eta = \left(\frac{2\Omega}{\nu_f}\right)^{1/2} z, \quad \theta(\eta) = \frac{T - T_\infty}{T_m - T_\infty}, \quad \phi(\eta) = \frac{C - C_\infty}{C_m - C_\infty}, \\ u = r\Omega f'(\eta), \quad v = r\Omega g(\eta), \quad w = -\left(2\Omega\nu_f\right)^{1/2} f(\eta) \tag{9}$$

3. Solution of the problem

Eq. (9) immediately fulfills the continuity equation Eq. (1) and Eqs. (2-5) will be in the subsequent form:

$$\frac{1}{A_1 A_2}(2f''' - \eta^* f') + 2ff'' - (1 + F_r)f'^2 \\ + g^2 - \frac{\sigma_{hnf}}{\sigma_f}\frac{M_1}{A_2} f' = 0, \tag{10}$$

$$\frac{1}{A_1 A_2}(2g'' - \eta^* g) - 2gf' + 2fg' \\ - F_r g^2 - \frac{\sigma_{hnf}}{\sigma_f}\frac{M_1}{A_2} g = 0, \tag{11}$$

$$\left(\frac{K_{hnf}}{K_f} + \frac{4}{3}Rd\right)\theta'' + A_3 Prf\theta' + \frac{1}{2}\beta Pr\theta \\ + \frac{1}{2}\frac{\sigma_{hnf}}{\sigma_f} M_1 Br(f'^2 + g^2) + \frac{Br}{A_1}(f''^2 + g'^2) \\ + A_2 \frac{D_{hnf}}{D_f} DuPr\phi'' = 0, \tag{12}$$

$$\frac{D_{hnf}}{D_f}\frac{1}{Sc}\phi'' + f\phi' + \frac{D_{hnf}}{D_f} Sr\theta'' = 0. \tag{13}$$

where,

$$A_1 = [(1 - \varphi_1)(1 - \varphi_2)]^{\frac{1}{2}}, \\ A_2 = \left[\varphi_1\left(\frac{\rho_{s1}}{\rho_f}\right) + (1 - \varphi_1)\right](1 - \varphi_2) + \varphi_2\left(\frac{\rho_{s2}}{\rho_f}\right), \\ A_3 = \left[\varphi_1\left(\frac{(\rho c_p)_{s1}}{(\rho c_p)_f}\right) + (1 - \varphi_1)\right](1 - \varphi_2) \\ + \varphi_2\left(\frac{(\rho c_p)_{s2}}{(\rho c_p)_f}\right) \tag{14}$$

The transformed boundary conditions are then given by:

$$f' = 0, \quad A_2 Prf + \frac{K_{hnf}}{K_f} Me\theta' = 0, \\ g = 1, \quad \theta = 1, \quad \phi = 1 \quad at \quad \eta = 0 \\ f' \to 0, \quad g \to 0, \quad \theta \to 0, \quad \phi \to 0 \quad as \quad \eta \to \infty \tag{15}$$

where, primes here denote differentiation concerning η.

The parameters used throughout for this model are defined as follows:

$$\eta^* = \frac{\nu_f}{\Omega k_1}, \quad F_r = \frac{C_b}{k_1^{\frac{1}{2}}}, \quad M_1 = \frac{\sigma_f B_0^2}{\Omega\rho_f}, \quad Rd = \frac{4\sigma^* T_\infty^2}{k^* K_f}, \\ Br = EcPr, \qquad Pr = \frac{\nu_f (\rho c_p)_f}{K_f}, \tag{16}$$

$$Ec = \frac{r^2\Omega^2}{(c_p)_f (T_m - T_\infty)}, \quad \beta = \frac{Q}{\Omega(\rho c_p)_f}, \\ Re = \left(\frac{\Omega r^2}{\nu_f}\right), \qquad Du = \frac{D_f K (C_m - C_\infty)}{Cs_1 (c_p)_f \nu_f (T_m - T_\infty)}, \\ Sr = \frac{D_f K (T_m - T_\infty)}{T_m \nu_f (C_m - C_\infty)}, \quad Sc = \frac{\nu_f}{D_f}.$$

The dimensionless melting parameter Me is defined as follows:

$$Me = \frac{(c_p)_f (T_\infty - T_m)}{\lambda_3 + Cs_2 (T_m - T_0)}. \tag{17}$$

Eq. 17 consists of a combination of the two Stefan numbers $(c_p)_f (T_\infty - T_m)/\lambda_3$ and $Cs_2 (T_m - T_0)/\lambda_3$ for the liquid and solid phases, respectively.

The local skin-friction coefficient C_{fx}, the local Sherwood number Sh and the local Nusselt number Nu are the relevant physical quantities and they are explained as follows (Imtiaz *et al*. 2019, Mahanthesh *et al*. 2019, M. G. Reddy *et al*. 2021):

$$C_{fx} = \frac{\sqrt{\tau_{wt}^2 + \tau_{w\phi}^2}}{\rho_f (\Omega r)^2}, \tag{18}$$

$$Sh = \frac{r j_w}{D_{hnf}(C_m - C_\infty)}, \tag{19}$$

$$Nu = \frac{r q_w}{K_f (T_m - T_\infty)}. \tag{20}$$

where, τ_{wt}, $\tau_{w\Phi}$, j_{wt}, and q_w are defined by:

$$\tau_{wt} = \left[\mu_{hnf}\left(\frac{\partial u}{\partial z} + \frac{\partial w}{\partial \Phi}\right)\right]_{z=0}, \\ \tau_{w\Phi} = \left[\mu_{hnf}\left(\frac{\partial v}{\partial z} + \frac{1}{r}\frac{\partial w}{\partial \Phi}\right)\right]_{z=0}, \\ j_w = -\left[D_{hnf}\left(\frac{\partial C}{\partial z}\right)\right]_{z=0}, \\ q_w = -\left[K_{hnf}\frac{\partial T}{\partial z}\right]_{z=0}. \tag{21}$$

We obtain the following relations after employing the similarity variables (Eq.9):

$$C_{fx} Re^{1/2} = \frac{1}{A_1}\sqrt{\left(f''(0)\right)^2 + \left(g'(0)\right)^2}, \tag{22}$$

$$ShRe^{-1/2} = -\phi'(0) \tag{23}$$

$$NuRe^{-1/2} = -\frac{K_{hnf}}{K_f}\theta'(0). \tag{24}$$

4. Solution Methodology

The domain of the controlling boundary layer equations, Eqs. (10-13), is $0 \le \eta \le \eta_\infty$, that η_∞ is defined as one end of the computational domain that the user specifies.

Utilizing the following algebraic mapping:

$$\chi = 2\frac{\eta}{\eta_\infty} - 1. \tag{25}$$

The unbounded region $(0,\infty)$ is translated into the finite domain $[-1,1]$, and the model represented by Eq.10 through Eq. (13) become incorporated into the following system:

$$\begin{aligned}&\left(\frac{2}{A_1A_2}\right)f'''(\chi) - \left(\frac{\eta_\infty}{2}\right)[f'^2(\chi) - 2f(\chi)f''(\chi) + F_r f'^2(\chi)]\\ &-\left(\frac{\eta_\infty}{2}\right)^2\left[\frac{\eta^*}{A_1A_2} + \frac{\sigma_{hnf}}{\sigma_f}\frac{M_1}{A_2}\right]f'(\chi) + \left(\frac{\eta_\infty}{2}\right)^3 g^2(\chi) = 0,\end{aligned} \tag{26}$$

$$\begin{aligned}&\left(\frac{2}{A_1A_2}\right)g''(\chi) + \left(\frac{\eta_\infty}{2}\right)[2f(\chi)g'(\chi) - 2g(\chi)f'(\chi)]\\ &-\left(\frac{\eta_\infty}{2}\right)^2\left[F_r g^2(\chi) + \left(\frac{\eta^*}{A_1A_2} + \frac{\sigma_{hnf}}{\sigma_f}\frac{M_1}{A_2}\right)g(\chi)\right] = 0,\end{aligned} \tag{27}$$

$$\begin{aligned}&\left(\frac{K_{hnf}}{K_f} + \frac{4}{3}Rd\right)\theta''(\chi) + \frac{\sigma_{hnf}}{\sigma_f}M_1 Br f'^2(\chi) + \frac{Br}{A_1}g'^2(\chi)\\ &+A_2\frac{D_{hnf}}{D_f}DuPr\phi''(\chi) + A_3 Pr\left(\frac{\eta_\infty}{2}\right)f(\chi)\theta'(\chi)\\ &+\frac{1}{2}\left(\frac{\eta_\infty}{2}\right)^2\left[\beta Pr\theta(\chi) + \frac{\sigma_{hnf}}{\sigma_f}M_1 Br g^2(\chi)\right]\\ &+\frac{Br}{A_1}\left(\frac{2}{\eta_\infty}\right)^2 f''^2(\chi) = 0,\end{aligned} \tag{28}$$

$$\frac{D_{hnf}}{D_f}\frac{1}{Sc}\phi''(\chi) + \frac{D_{hnf}}{D_f}Sr\theta''(\chi) + \left(\frac{\eta_\infty}{2}\right)f(\chi)\phi'(\chi) = 0. \tag{29}$$

The modified boundary conditions come from:

$$\begin{aligned}&A_2 Prf(-1) + \frac{K_{hnf}}{K_f}\left(\frac{2}{\eta_\infty}\right)Me\theta'(-1) = 0,\\ &f'(-1) = 0, \quad g(-1) = 1, \quad f'(1) = 0,\\ &g(1) = 0, \quad \theta(-1) = 1, \quad \theta(1) = 0,\\ &\phi(-1) = 1, \quad \phi(1) = 0.\end{aligned} \tag{30}$$

By beginning with a Chebyshev approximation for the highest-order derivatives, f''', g'', θ'' and ϕ'' and then producing approximations to the lower-order derivatives f'', f', f, g', g, θ', θ, ϕ' and ϕ as follows:

Setting $f''' = \psi(\chi)$, $g'' = \delta(\chi)$, $\theta'' = \zeta(\chi)$ and $\phi'' = \varsigma(\chi)$, then by integration, we get:

$$f''(\chi) = \int_{-1}^{\chi}\psi(\chi)d\chi + C_1^f, \tag{31}$$

$$f'(\chi) = \int_{-1}^{\chi}\int_{-1}^{\chi}\psi(\chi)d\chi d\chi + C_1^f(\chi+1) + C_2^f, \tag{32}$$

$$\begin{aligned}f(\chi) = \int_{-1}^{\chi}\int_{-1}^{\chi}\int_{-1}^{\chi}\psi(\chi)d\chi d\chi d\chi + C_1^f\frac{(\chi+1)^2}{2}\\ + C_2^f(\chi+1) + C_3^f,\end{aligned} \tag{33}$$

$$g'(\chi) = \int_{-1}^{\chi}\delta(\chi)d\chi + C_1^g, \tag{34}$$

$$g(\chi) = \int_{-1}^{\chi}\int_{-1}^{\chi}\delta(\chi)d\chi d\chi + C_1^g(\chi+1) + C_2^g, \tag{35}$$

$$\theta'(\chi) = \int_{-1}^{\chi}\zeta(\chi)d\chi + C_1^\theta, \tag{36}$$

$$\theta(\chi) = \int_{-1}^{\chi}\int_{-1}^{\chi}\zeta(\chi)d\chi d\chi + C_1^\theta(\chi+1) + C_2^\theta, \tag{37}$$

$$\phi'(\chi) = \int_{-1}^{\chi}\varsigma(\chi)d\chi + C_1^\phi, \tag{38}$$

$$\phi(\chi) = \int_{-1}^{\chi}\int_{-1}^{\chi}\varsigma(\chi)d\chi d\chi + C_1^\phi(\chi+1) + C_2^\phi. \tag{39}$$

From the boundary condition Eq. 30, we obtain:

$$\begin{aligned}&C_1^f = -\frac{1}{2}\int_{-1}^{1}\int_{-1}^{\chi}\psi(\chi)d\chi d\chi,\\ &C_2^f = 0,\\ &C_3^f = -\frac{Me}{A_2Pr}\frac{K_{hnf}}{K_f}\left(\frac{2}{\eta_\infty}\right)\left[-\frac{1}{2} - \frac{1}{2}\int_{-1}^{1}\int_{-1}^{\chi}\zeta(\chi)d\chi d\chi\right],\\ &C_1^g = -\frac{1}{2}\int_{-1}^{1}\int_{-1}^{\chi}\delta(\chi)d\chi - \frac{1}{2},\\ &C_2^g = 1,\\ &C_1^\theta = -\frac{1}{2}\int_{-1}^{1}\int_{-1}^{\chi}\zeta(\chi)d\chi d\chi - \frac{1}{2},\\ &C_2^\theta = 1,\\ &C_1^\phi = -\frac{1}{2}\int_{-1}^{1}\int_{-1}^{\chi}\varsigma(\chi)d\chi d\chi - \frac{1}{2},\\ &C_2^\phi = 1.\end{aligned} \tag{40}$$

Therefore, we can give approximations to Eqs.(31)-(39) as following form:

$$\begin{aligned}f_i(\chi) &= \sum_{j=0}^{N}\left(l_{ij}^f\psi_j + l_{ij}^{\bar{f}}\zeta_j\right) + d_i^f,\\ f_i'(\chi) &= \sum_{j=0}^{N}\left(l_{ij}^{f1}\psi_j + l_{ij}^{\bar{f}1}\zeta_j\right) + d_i^{f1},\\ f_i''(\chi) &= \sum_{j=0}^{N}\left(l_{ij}^{f2}\psi_j + l_{ij}^{\bar{f}2}\zeta_j\right) + d_i^{f2},\end{aligned} \tag{41}$$

$$g_i(\chi) = \sum_{j=0}^{N}l_{ij}^g\delta_j + d_i^g, \quad g_i'(\chi) = \sum_{j=0}^{N}l_{ij}^{g1}\delta_j + d_i^{g1}, \tag{42}$$

$$\theta_i(\chi) = \sum_{j=0}^{N}l_{ij}^\theta\zeta_j + d_i^\theta, \quad \theta_i'(\chi) = \sum_{j=0}^{N}l_{ij}^{\theta1}\zeta_j + d_i^{\theta1}, \tag{43}$$

$$\phi_i(\chi) = \sum_{j=0}^{N}l_{ij}^\phi\varsigma_j + d_i^\phi, \quad \phi_i'(\chi) = \sum_{j=0}^{N}l_{ij}^{\phi1}\varsigma_j + d_i^{\phi1}. \tag{44}$$

for all $i = 0(1)N$, such that,

$$l_{ij}^\phi = b_{ij}^2 - \frac{(\chi_i+1)}{2}b_{Nj}^2, \quad d_i^\phi = -\frac{(\chi_i+1)}{2} + 1, \tag{45}$$

$$l_{ij}^{\phi 1} = b_{ij} - \frac{1}{2}b_{Nj}^2, \quad d_i^{\phi 1} = -\frac{1}{2},$$
$$l_{ij}^{\theta} = b_{ij}^2 - \frac{(\chi_i+1)}{2}b_{Nj}^2, \quad d_i^{\theta} = -\frac{(\chi_i+1)}{2}+1,$$
$$l_{ij}^{\theta 1} = b_{ij} - \frac{1}{2}b_{Nj}^2, \quad d_i^{\theta 1} = -\frac{1}{2},$$
$$l_{ij}^{g} = b_{ij}^2 - \frac{(\chi_i+1)}{2}b_{Nj}^2, \quad d_i^{g} = -\frac{(\chi_i+1)}{2}+1,$$
$$l_{ij}^{g 1} = b_{ij} - \frac{1}{2}b_{Nj}^2, \quad d_i^{g 1} = -\frac{1}{2},$$
$$l_{ij}^{f} = b_{ij}^3 - \frac{(\chi_i+1)^2}{4}b_{Nj}^2, \quad l_{ij}^{\bar{f}} = \frac{Me}{2A_2Pr}\frac{K_{hnf}}{K_f}\left(\frac{2}{\eta_\infty}\right)b_{Nj}^2,$$
$$d_i^{f} = \frac{Me}{2A_2Pr}\frac{K_{hnf}}{K_f}\left(\frac{2}{\eta_\infty}\right), \quad l_{ij}^{f1} = b_{ij}^2 - \frac{(\chi_i+1)}{2}b_{Nj}^2,$$
$$l_{ij}^{\bar{f}1} = 0, \quad d_i^{f1} = 0, \quad l_{ij}^{f2} = b_{ij} - \frac{1}{2}b_{Nj}^2,$$
$$l_{ij}^{\bar{f}2} = 0, \quad d_i^{f2} = 0.$$

where $\chi_i = -cos\left(\frac{i\pi}{N}\right)$ are the Chebyshev points, and b_{ij} are the elements of the matrix B, according to (El-gendi 1969):

$$b_{ij}^2 = (\chi_i - \chi_j)b_{ij}. \tag{46}$$

We can transform Eqs. (26-30) by using Eqs. (41-44) to the following system of non-linear equations in the highest derivatives into the following Chebyshev spectral equations:

$$\left(\frac{2}{A_1A_2}\right)\delta_i + \left(\frac{\eta_\infty}{2}\right)\begin{bmatrix} 2\left(\sum_{j=0}^{N}\left(l_{ij}^{f}\psi_j + l_{ij}^{\bar{f}}\zeta_j\right) + d_i^{f}\right) \\ \left(\sum_{j=0}^{N} l_{ij}^{g1}\delta_j + d_i^{g1}\right)\end{bmatrix}$$
$$\left(\frac{\eta_\infty}{2}\right)\begin{bmatrix} -2\left(\sum_{j=0}^{N} l_{ij}^{g}\delta_j + d_i^{g}\right) \\ \left(\sum_{j=0}^{N}\left(l_{ij}^{f1}\psi_j + l_{ij}^{\bar{f}1}\zeta_j\right) + d_i^{f1}\right)\end{bmatrix}$$
$$-\left(\frac{\eta_\infty}{2}\right)^2\begin{bmatrix} F_r\left(\sum_{j=0}^{N} l_{ij}^{g}\delta_j + d_i^{g}\right)^2 \\ +\left(\frac{\eta^*}{A_1A_2} + \frac{\sigma_{hnf}}{\sigma_f}\frac{M_1}{A_2}\right)\left(\sum_{j=0}^{N} l_{ij}^{g}\delta_j + d_i^{g}\right)\end{bmatrix} = 0, \tag{47}$$

$$\left(\frac{2}{A_1A_2}\right)\delta_i + \left(\frac{\eta_\infty}{2}\right)\begin{bmatrix} 2\left(\sum_{j=0}^{N}\left(l_{ij}^{f}\psi_j + l_{ij}^{\bar{f}}\zeta_j\right) + d_i^{f}\right) \\ \left(\sum_{j=0}^{N} l_{ij}^{g1}\delta_j + d_i^{g1}\right)\end{bmatrix}$$
$$\left(\frac{\eta_\infty}{2}\right)\begin{bmatrix} -2\left(\sum_{j=0}^{N} l_{ij}^{g}\delta_j + d_i^{g}\right) \\ \left(\sum_{j=0}^{N}\left(l_{ij}^{f1}\psi_j + l_{ij}^{\bar{f}1}\zeta_j\right) + d_i^{f1}\right)\end{bmatrix}$$
$$-\left(\frac{\eta_\infty}{2}\right)^2\begin{bmatrix} F_r\left(\sum_{j=0}^{N} l_{ij}^{g}\delta_j + d_i^{g}\right)^2 \\ +\left(\frac{\eta^*}{A_1A_2} + \frac{\sigma_{hnf}}{\sigma_f}\frac{M_1}{A_2}\right)\left(\sum_{j=0}^{N} l_{ij}^{g}\delta_j + d_i^{g}\right)\end{bmatrix} = 0, \tag{48}$$

$$\left(\frac{K_{hnf}}{K_f} + \frac{4}{3}Rd\right)\zeta_i + \frac{1}{2}\frac{\sigma_{hnf}}{\sigma_f}M_1Br\left(\sum_{j=0}^{N}\left(l_{ij}^{f1}\psi_j + l_{ij}^{\bar{f}1}\zeta_j\right) + d_i^{f1}\right)^2$$
$$+A_2\frac{D_{hnf}}{D_f}DuPr\varsigma_i + \frac{Br}{A_1}\left(\sum_{j=0}^{N} l_{ij}^{g1}\delta_j + d_i^{g1}\right)^2$$
$$+A_3Pr\left(\frac{\eta_\infty}{2}\right)\left[\left(\sum_{j=0}^{N}\left(l_{ij}^{f}\psi_j + l_{ij}^{\bar{f}}\zeta_j\right) + d_i^{f}\right)\left(\sum_{j=0}^{N} l_{ij}^{\theta 1}\zeta_j + d_i^{g1}\right)\right]$$
$$+\left(\frac{\eta_\infty}{2}\right)^2\left[\frac{1}{2}\beta Pr\left(\sum_{j=0}^{N} l_{ij}^{\theta}\zeta_j + d_i^{\theta}\right) + \frac{1}{2}\frac{\sigma_{hnf}}{\sigma_f}M_1Br\left(\sum_{j=0}^{N} l_{ij}^{g}\delta_j + d_i^{g}\right)^2\right]$$
$$+\frac{Br}{A_1}\left(\frac{2}{\eta_\infty}\right)^2\left(\sum_{j=0}^{N}\left(l_{ij}^{f2}\psi_j + l_{ij}^{\bar{f}2}\zeta_j\right) + d_i^{f2}\right)^2 = 0. \tag{49}$$

$$\frac{D_{hnf}}{D_f}\left(\frac{1}{Sc}\varsigma_i + Sr\zeta_i\right)$$
$$+\left(\frac{\eta_\infty}{2}\right)\left[\left(\sum_{j=0}^{N}\left(l_{ij}^{f}\psi_j + l_{ij}^{\bar{f}}\zeta_j\right) + d_i^{f}\right)\left(\sum_{j=0}^{N} l_{ij}^{\phi 1}\varsigma_j + d_i^{\phi 1}\right)\right] = 0. \tag{50}$$

The computer program was run on a PC using Mathematica 12 to solve this system using Newton's iteration technique with $N = 12$.

5. Results Interpretation

The main goal in this section is to comprehend how certain parameters can significantly impact flow fields, heat, and mass transfer. In a steady incompressible 3-D Darcy-Forchheimer hybrid Nanofluid flow "with s=3" incorporating melting heat transfer over a rotating disk, we have obtained the numerical solution for the radial velocity of both fluid $f'(\eta)$ and tangential velocity $g(\eta)$, temperature $\theta(\eta)$, concentration $\phi(\eta)$, skin friction number C_{fx}, Nusselt Number Nu, and Sherwood Number Sh by using the Chebyshev spectral technique. The analysis is carried out to understand the impact of periodic body acceleration via the pertinent normalized physical parameters, namely magnetic parameter M_1, porosity parameter η^*, radiation parameter Rd, Forchhiemer number F_r, volume concentration φ_1, Dufour number Du, Brinkman number Br, Schmidt number Sc, heat generation absorption parameter β, Prandtl number Pr, Eckert number Ec, Soret number Sr, volume concentration φ_2, and melting parameter Me. The physical variations in velocity profiles of fluid, temperature distribution, concentration, skin friction number, Nusselt Number, and Sherwood Number concerning transformed coordinates are analyzed and discussed through the Figs. 4-12 and Tables 2-4. For the numerical computation, the dimensionless values of the physical parameters are used as available in the scientific literature.

Table 1 demonstrates the characteristics of nanoparticles and explains the nanoparticle's and each base fluid's thermophysical characteristics.

Table 2 indicates the variations of the numerical values of skin friction coefficient $Re^{0.5}C_{fx}$ for various quantities of physical parameters M_1, η^*, φ_1, and φ_2. It is obvious that the comparison of nanofluid and hybrid nanofluid

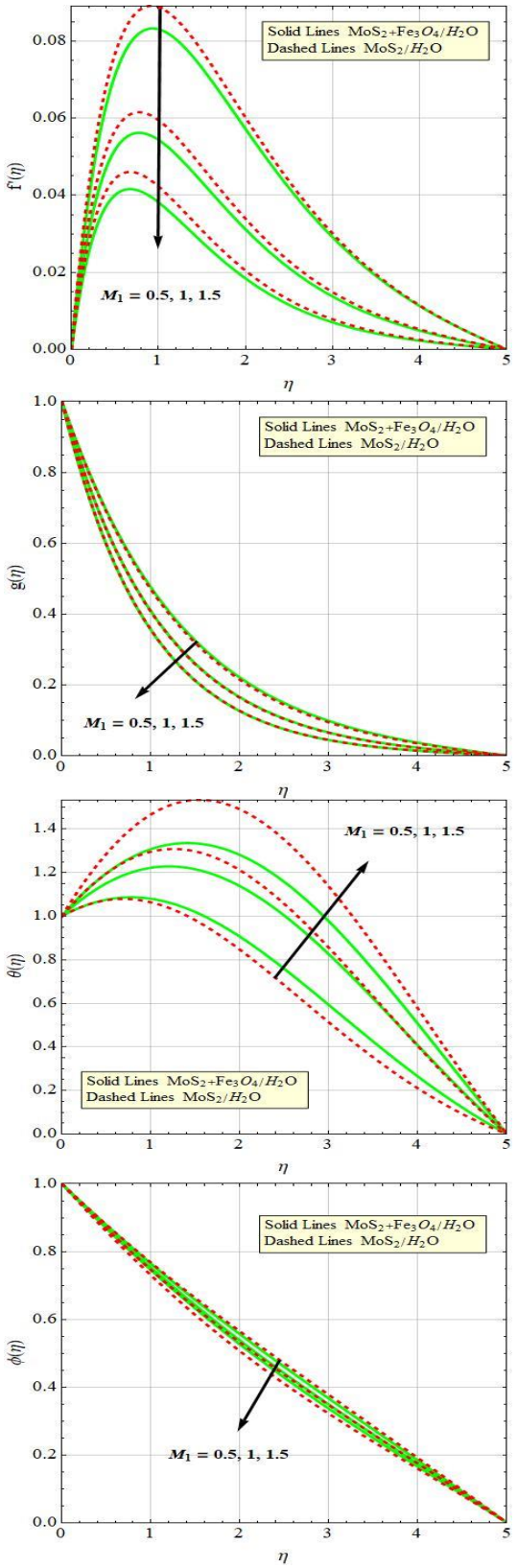

Fig. 4 Consequence of M_1 on $f'(\eta)$, $g(\eta)$, $\theta(\eta)$, $\phi(\eta)$

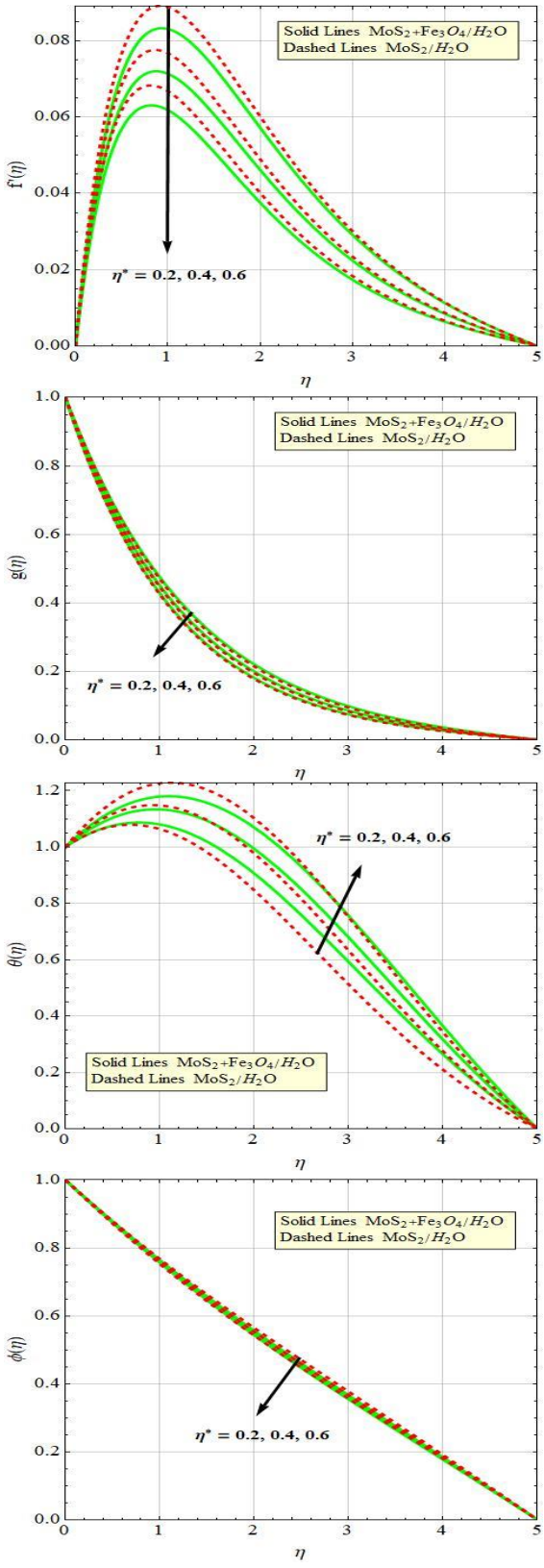

Fig. 5 Consequence of η^* on $f'(\eta)$, $g(\eta)$, $\theta(\eta)$, $\phi(\eta)$

results in the skin friction coefficient, and the numerical values of skin friction coefficient of both hybrid nanofluid (MoS_2+Fe_3O_4/H_2O) and nanofluid (MoS_2/H_2O) are enhanced for different values of M_1, η^*, and φ_1, while the numerical values of skin friction coefficients are decreasing for different values of φ_2. It is noticed that the skin friction coefficient is increased for larger values of M_1, η^*, φ_1, while it reduced for increasing φ_2.

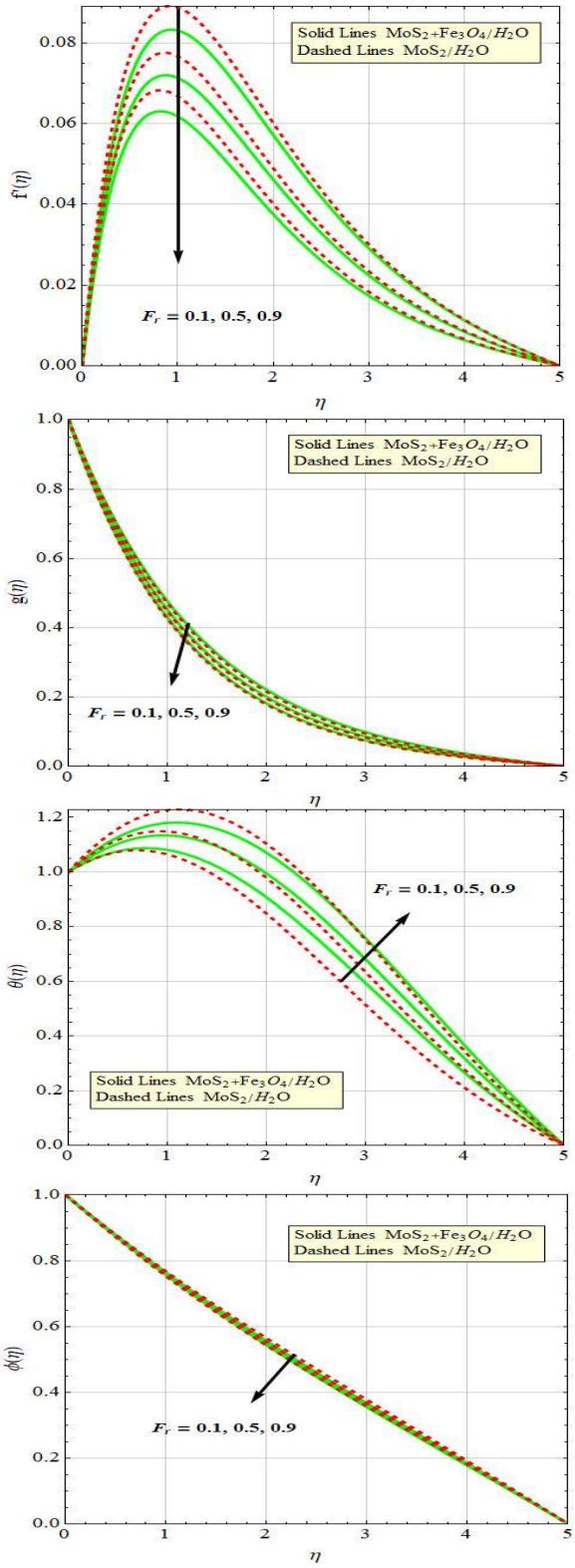

Fig. 6 Consequence of F_r on $f'(\eta)$, $g(\eta)$, $\theta(\eta)$, $\phi(\eta)$

From Table 3, the heat transfer rate scale-back value can be estimated by adding all the values of Me, Br, φ_1, and φ_2. It displays the variations of the numerical values of Nusselt number $Re^{0.5}Nu$ for various quantities of physical parameters as mentioned. It is obvious that the Nusselt number is increasing function as Me and Br rise while a reverse trend is detected for booster values of both φ_1 and φ_2.

Table 1 Values of thermo-physical properties for base fluid and nanoparticles (Reddy *et al.* 2021)

Physical properties	Base fluid	Nanoparticles	
	Water (H_2O)	Molybdenum disul-fide (MoS_2)	Iron (II,III) oxide (Fe_3O_4)
Density (ρ) (kg m^{-3})	997.1	5060	5180
Specific heat (C_p) (J (kg K)$^{-1}$)	4179	397	670
Thermal conductivity (K) (W m K^{-1})	0.613	904.4	9.7
Electrical conductivity (σ) (s m^{-1})	5.5 × 10^{-6}	2090	25000

Table 2 Numerical values of skin friction "$Re^{0.5}\,C_{fx}$" for various quantities of physical parameters

				$Re^{0.5}\,C_{fx}$	
M_1	η^*	φ_1	φ_2	Nanofluid	Hybrid nanofluid
0.5				1.009996	1.289544
1.0				1.188397	1.537888
1.5				1.359251	1.770786
	0.2			1.009996	1.289544
	0.4			1.071889	1.374389
	0.6			1.134069	1.458826
		0.1		1.893133	1.857393
		0.2		1.944288	1.888371
		0.3		1.990837	1.941693
			0.1	1.794861	1.857393
			0.2	1.760780	1.791498
			0.3	1.684984	1.699841

Table 3 Numerical values of Nusselt number "$Re^{-0.5}$ Nu" for various quantities of physical parameters

				$Re^{-0.5}$ Nu	
Me	η^*	φ_1	φ_2	Nanofluid	Hybrid nanofluid
0				−0.344736	−0.336970
0.05				−0.351839	−0.341717
0.1				−0.359184	−0.346557
	0.1			−0.346137	−0.337912
	0.5			−0.581757	−0.592894
	0.9			−0.817311	−0.847788
		0.1		−0.920307	−0.898438
		0.2		−0.448233	−0.409860
		0.3		−0.062542	−0.019693
			0.1	−0.812953	−0.450337
			0.2	−0.696406	−0.381353
			0.3	−0.559015	−0.297300

Table 4 Numerical values of Sherwood number "$Re^{-0.5}\,Sh$" for various quantities of physical parameters

				$Re^{-0.5}\,Sh$	
Du	Pr	φ_1	φ_2	Nanofluid	Hybrid nanofluid
0				0.248157	0.249619
0.2				0.251206	0.250702
0.4				0.254640	0.250857
	6			0.249638	0.250580
	7			0.257542	0.259808
	8			0.265453	0.270173
		0.1		0.249638	0.250580
		0.2		0.239524	0.239980
		0.3		0.231280	0.231325
			0.1	0.267058	0.250580
			0.2	0.263267	0.249159
			0.3	0.259205	0.247729

Table 4 shows the variations of the numerical values of Sherwood number $Re^{0.5}Sh$ for various quantities of physical parameters Du, Pr, φ_1, and φ_2. It is obvious that the rate of mass transfer increased for increasing values of Du and Pr, while it declined for increasing values of both φ_1 and φ_2.

The variations in radial velocity profiles $f'(\eta)$, tangential velocity profiles $g(\eta)$, dimensionless temperature $\theta(\eta)$, and dimensionless concentration $\phi(\eta)$ of Darcy-Forchheimer flow at the two abnormal sections (hybrid nanofluid and nanofluid) with the varying magnitudes of the magnetic parameter M_1, porosity parameter η^*, Forchhiemer parameter F_r are illustrated in Figs. 4-6. It is clear from these figures that both the radial velocity profiles, tangential velocity, temperature, and concentration are zero near the disk wall, which endorses the no-slip boundary condition and enhances to a maximum value near the central axis of the disk. It is also important to note that the hybrid nanofluid (HNF) moves slower than the nanofluid (NF) because of the drag force for both radial and tangential velocity as well as temperature. It is found that, the radial velocity, tangential velocity, and concentration decrease with increasing of M_1, η^*, and F_r, as well the temperature increases with increasing of M_1, η^*, and F_r. Physically, the dimensionless velocities usually decrease substantially as the magnetic field increases. This is due to the Lorentz force, a body force that retards, being introduced by the magnetic field. This results from an electrically conducting fluid's velocity interacting with the magnetic and electric fields. That is, because a magnetic field exists physically, a resistive force forms in the flow of the nanofluid. This force can reduce the speed of both nanofluid and hybrid nanofluid. Moreover, the fluid interacts with the porous substance, increasing its viscosity and generating resistance, which reduces the fluid's speed. That is to say, it should be remembered that the same parameter F_r grows, an obstructive force acts against both the boundary layer's thickness and velocity. The plots reveal the quantitative

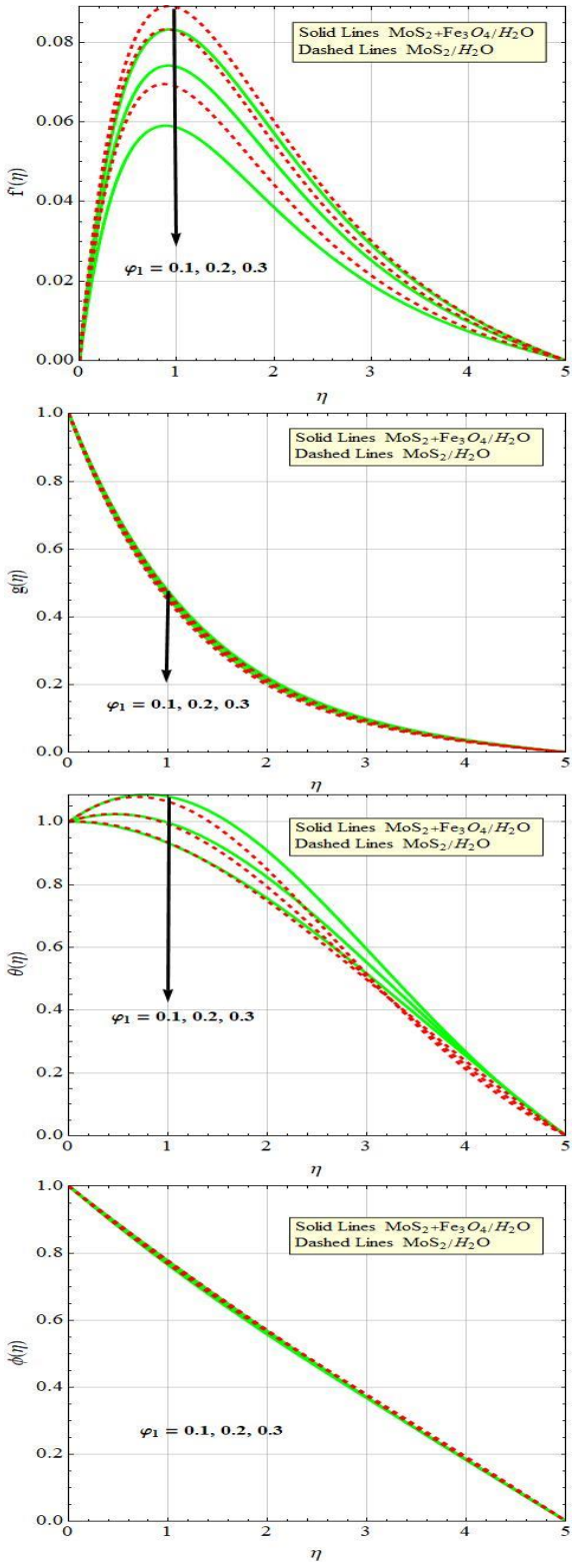

Fig. 7 Consequence of φ_1 on $f'(\eta)$, $g(\eta)$, $\theta(\eta)$, $\phi(\eta)$

difference between the results obtained by the present analysis results and by (Rashid *et al*. 2023).

Fig. 7 demonstrates the impact of volume concentration φ_1 on radial velocity profiles, tangential velocity, temperature, and concentration. It is observed that the radial velocity profiles, tangential velocity, temperature, and

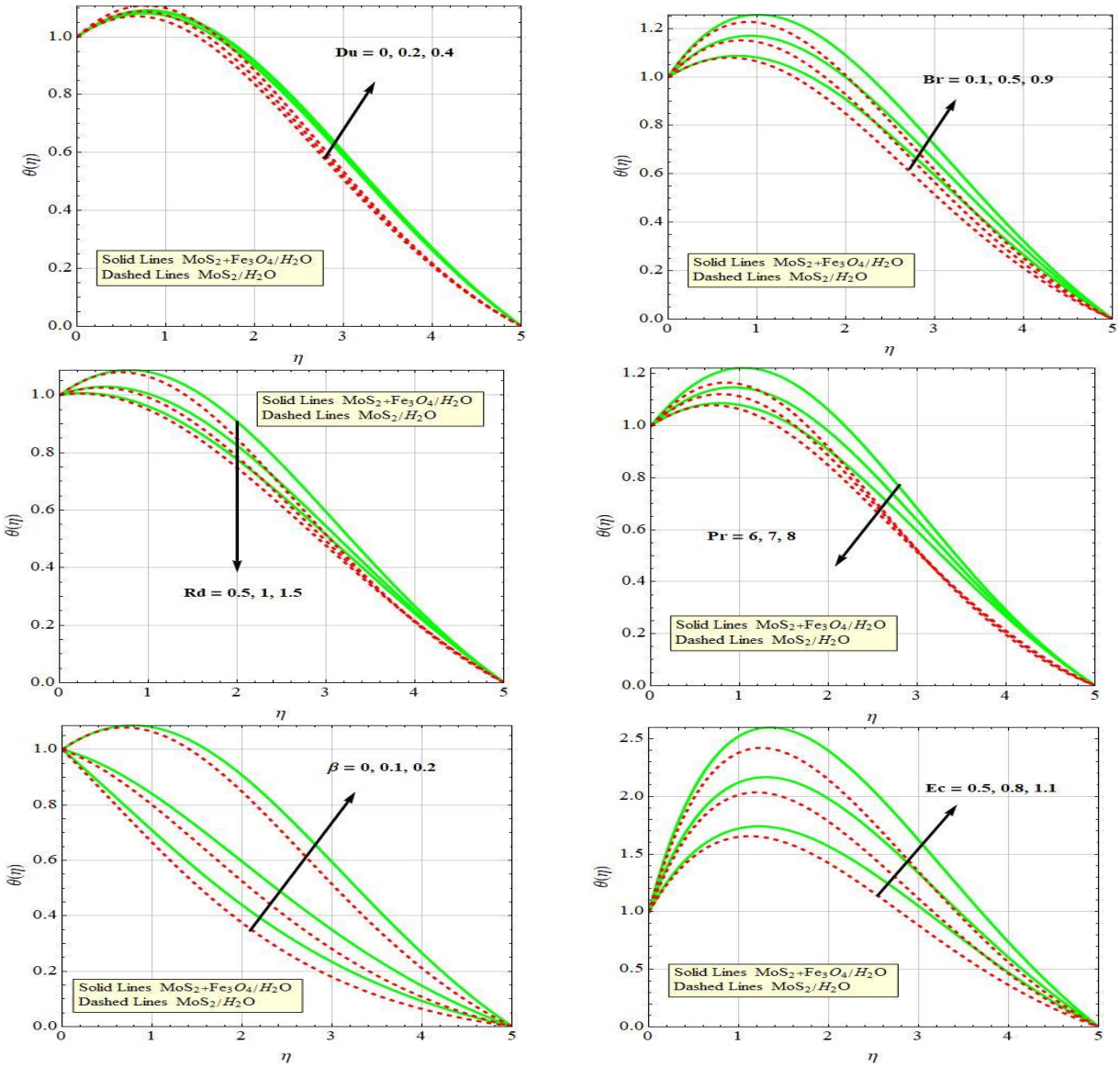

Fig. 8 Consequence of Du, Br, Rd, Pr, β, and Ec on $\theta(\eta)$.

concentration decrease as it increases the volume concentration. It is clear from these figures that both radial velocity profiles, tangential velocity, temperature, and concentration are zero near the disk wall, which endorses the no-slip boundary condition and enhances to a maximum value near the central axis of the disk. It is also important to note that the hybrid nanoparticle fluid moves slower than the nanoparticle fluid because of the drag force for both radial velocity and temperature, while the radial velocity, tangential velocity, temperature, and concentration decrease with increasing of φ_1. The higher the volume concentration of hybrid nanoparticles, the lesser the magnitude of the radial velocity profiles, tangential velocity, temperature, and concentration respectively display the results obtained in the present analysis and that of (Islam *et al*. 2023).

Fig. 8 presented the behavior analysis of dimensionless temperature profiles $\theta(\eta)$ against the transformed coordinates η subject to Dufour number Du, Brinkman number Br, radiation parameter Rd, Prandtl number Pr, heat generation absorption parameter β, and Eckert number Ec. This figure clearly shows that the temperature is zero near the disk wall, which endorses the no-slip boundary condition and enhances to a maximum value near the central axis of the disk. It is also important to note that the nanoparticle fluid moves slower than the hybrid nano-particle fluid because of the drag force for temperature. The temperature increases with increasing of Du, Br, β, and Ec, as well it decreases with increasing Rd and Pr. The thermal field grows as the Eckert number rises. An intriguing outcome in the case of a big magnetic force system is the significant disruption of the temperature field caused by each member. The combined effect of the heat energy stored in the nanofluid and hybrid nanofluid as a result of fractional heating is responsible for these physical phenomena. Substantially, the thermal field grows as the Eckert number rises. An intriguing outcome in the case of a big magnetic force system is the considerable disruption of the temperature field caused by each member. The combined effect of heat energy stored in the nanofluid and hybrid nanofluid as a result of fractional heating responsible

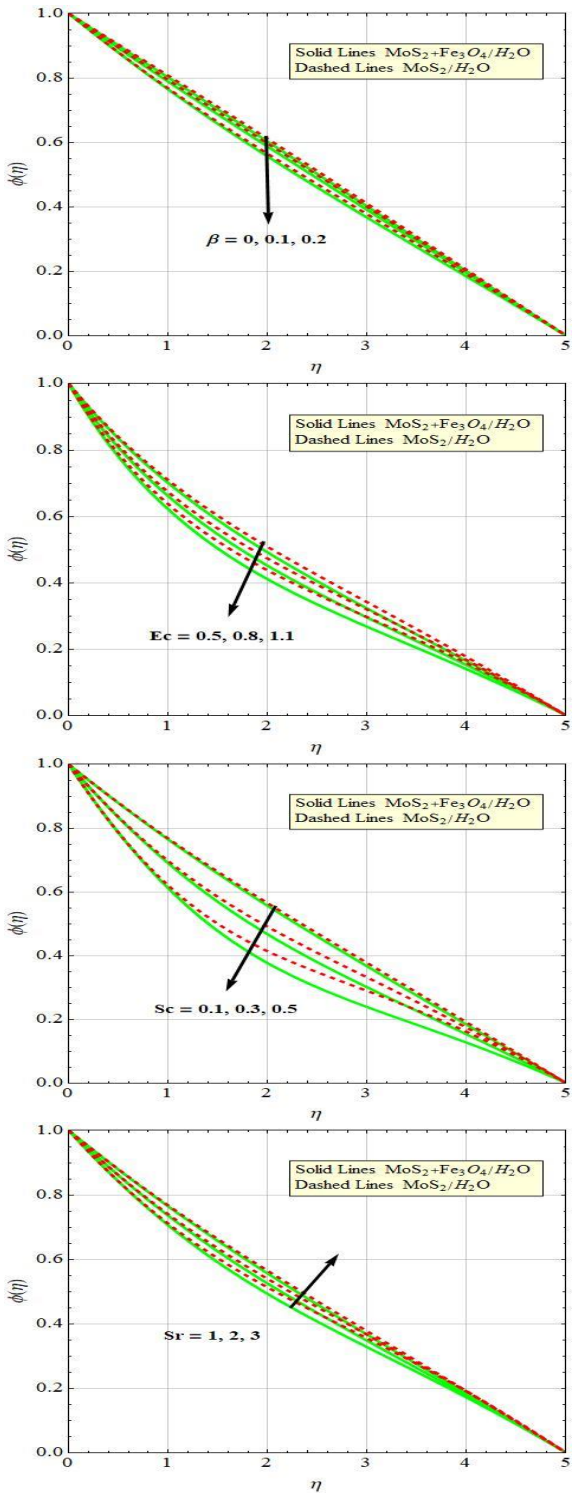

Fig. 9 Consequence of β, Ec, Sc, and Sr on $\phi(\eta)$

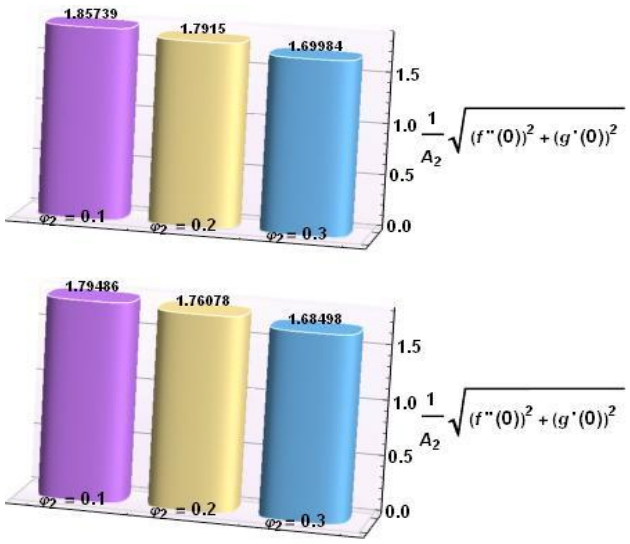

Fig. 10 Bar chart depiction of skin friction on φ_2

for these physical phenomena. Additionally, for Pr, the graph demonstrates that anytime the Pr values are increased, the thermal field and thermal layer thickness decrease. This is mostly because fluids with higher Prandtl numbers will have relatively low conductivities, which reduces heat transfer and the thickness of thermal fluid flow, ultimately lowering the fluid's temperature. Several research, including (Reddy *et al*. 2021, Shoaib *et al*. 2021), corroborate the findings of the current investigation. Some research, including, corroborate the findings of the current investigation. In contrast, the heat received by liquid particles from hot discs reduces the hybrid nanoparticles fluid between them. That results in an increase in the thickness of the thermal wall disk, an increase in the size of the temperature distribution, and a decline in the rate of heat transfer. This outcome means that increasing material fluid parameter values is more appropriate for cooling reasons.

Fig. 9 presented the behavior analysis of dimensionless $\phi(\eta)$ concentration profile against the transformed coordinates η subject to heat generation absorption parameter β, Eckert number Ec, Schmidt number Sc, and Soret number Sr. This figure shows clearly that the concentration is zero near the disk wall, which endorses the no-slip boundary condition and enhances to a maximum value near the central axis of the disk. Furthermore, in the case of nanoparticles, the fluid concentration occurs far faster than in the hybrid nanoparticle situation. While the proportion falls as the amount of β, Ec, and Sc but rises for Sr. The solutal layer of the nanoparticle and hybrid nanoparticle case declines for higher values of Sc. Since Sc is the ratio of kinematic viscosity to mass diffusivity, mass diffusivity becomes lower for larger Sc. As a result, the concentration profiles and its layer thickness are declined. It is important to note that the extreme values of Sc scale back the fluid concentration in this situation. It is important to note that the fluid concentration is scaled back by the extreme values of Sc An analogous observation was noted by (Reddy *et al*. 2021). The Soret effect is the name given to the thermodiffusion's reciprocal trend. That is the result of a temperature gradient on mass flux. In this case, the Soret parameter Sr is directly proportional to the concentration field. Consequently, it may be said that the cross-diffusion effect can be used to regulate the rate of heat mass transfer. Several research, including this one, provide support for the findings of the current investigation (Khan *et al*. 2022, Mahanthesh *et al*. 2019, Patil *et al*. 2023). All these concentration graphs reveal a graphical outcome and the concentration is minimum near the disk wall.

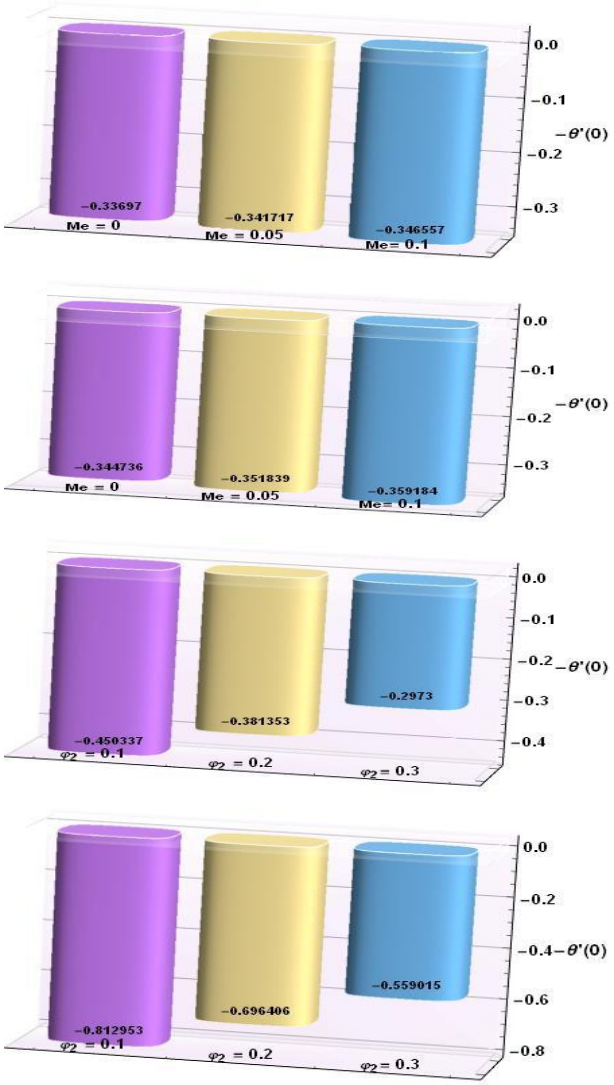

Fig. 11 Bar chart depiction of Nusselt Number on Me and φ_2

Fig. 10 shows the difference in the bar chart for a reduction in skin friction. $Re^{0.5}C_{fx}$ against the various values of volume concentration φ_2. It is observed that the skin friction drops as the amount of φ_2 for both (HNF) and (NF) cases. It is also important to note that the nanoparticle fluid moves slower than the hybrid nanoparticle fluid because of the drag force for skin friction.

Fig. 11 shows the bar chart variation for the rise in Nusselt number $Re^{0.5}Nu$ against the various values of melting parameter Me and a fall in volume concentration φ_2. The Nusselt number is seen to increase as the amount of Me declines for φ_2. It is also important to note that the nanofluid moves slower than the hybrid nanofluid because of the drag force for the Nusselt number.

Fig. 12 provides the bar chart representation for Sherwood Number $Re^{0.5}Sh$ against different values of Dufour number Du Prandtl number Pr and volume concentration φ_2, respectively. The Sherwood Number is noticed to rise with an increase in Du and Pr, while it falls as the amount of φ_2. It is also important to note that

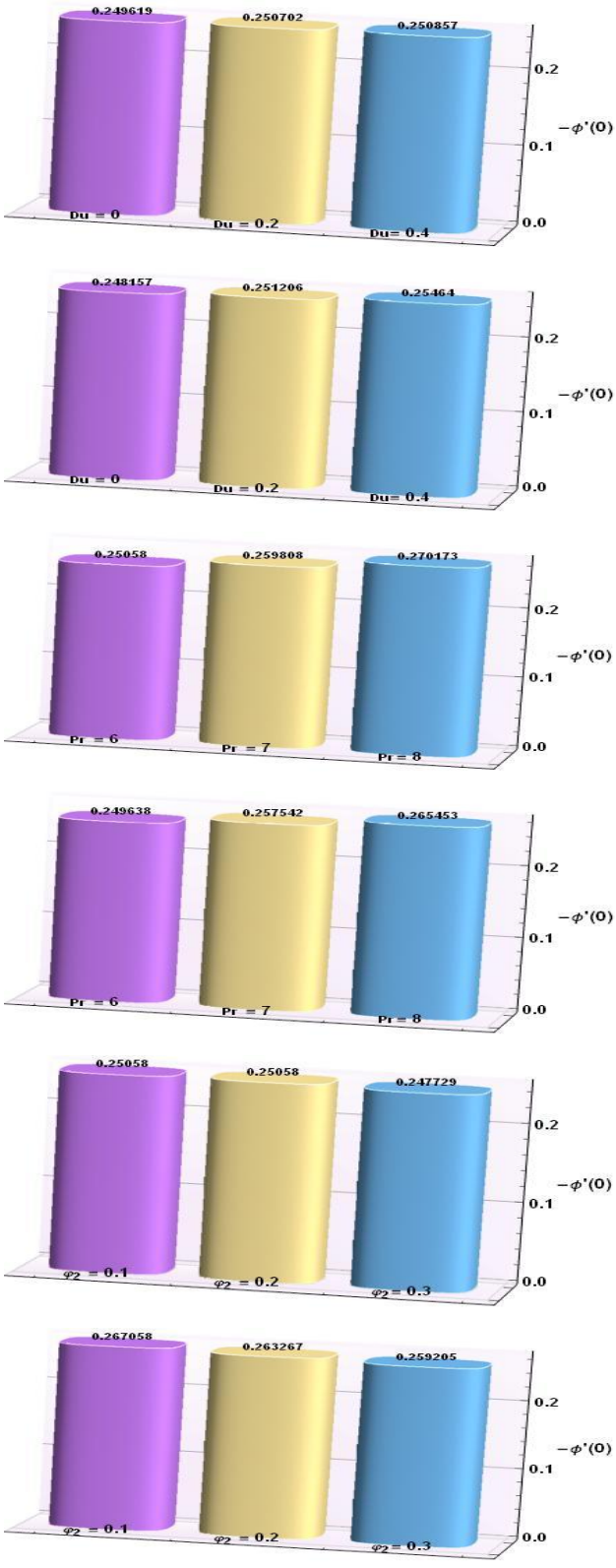

Fig. 12 Bar chart depiction of Sherwood Number on Du, Pr and φ_2

the nanofluid moves slower than the hybrid nanofluid. This bar chart depiction is now pushed ahead along with the boundary layer over the disk. This leads us to infer that bar chart depictions take place at high flow rates.

6. Conclusions

In this research, thermal radiation from a hybrid "$MoS_2 - Fe_3O_4/H_2O$" nanofluid flow carried by a Darcy-Forchheimer flow is examined over a rotating disc model with melting heat and mass transfer due to the substantial impact of magnetic nanoparticles. The governing issues have been converted into (ODEs) models by selecting the relevant symmetry variables, and the models are then solved numerically using the Chebyshev spectral approach. Principal findings include the following:

• One finding is that the radial velocity and tangential velocity of the nanoparticle exceed that of the hybrid nanoparticle almost everywhere. However, at the wall, the radial velocity and tangential velocity of the fluid are zero due to the imposition of the no-slip condition.

• The fluid radial velocity and tangential velocity downturns when the magnetic parameter, Forchheimer parameter, and porosity parameter rise.

• The skin friction coefficient of hybrid nanofluid is greater than nanofluid for different values of M_1, η^*, and φ_1.

• While radial and tangential velocities decrease with increasing M_1 values, a revised behavior in the temperature profile has been seen.

• Both the bar chart variation for skin friction, Nusselt number, and Sherwood number decline with the large values of φ_2.

• In comparison to the nanofluid, the hybrid nanofluid has a greater skin friction coefficient and Nusselt number.

• The Nusselt Number, which measures the rate of heat transport, has a decreasing trend as both volume concentration φ_1 and φ_2 rise.

• Extensive analysis of characteristics of relevance demonstrates that hybrid nanofluids are essential for fluid transfer and achieve a higher temperature distribution.

• The findings broadly agreed with the most recent and cutting-edge research that had been disclosed in the literature. It was stated that the current findings might advance engineering, fluid mechanics, and the biological sciences.

More aspects of the 3-D flow of hybrid nanofluid over a rotating disk under different influences may be explored in the future using increasingly sophisticated numerical computation methods employing artificial intelligence techniques.

Acknowledgment

The authors extend their appreciation to the Deputyship for Research & Innovation, Ministry of Education in Saudi Arabia for funding this research work through the project number 445-9-917.

References

Ajeel, R.K., Salim, W.S.I.W. and Hasnan, K. (2019), "Thermal performance comparison of various corrugated channels using nanofluid: numerical study", *Alexandria Eng J*., **58**(1), 75-87. https://doi.org/10.1016/j.aej.2018.12.009.

Ajeel, R.K., Salim, W.S.I.W. and Hasnan, K. (2019), "Thermal performance comparison of various corrugated channels using nanofluid: Numerical study", *Alexandria Eng J*., **58**(1), 75-87. https://doi.org/10.1016/j.aej.2018.12.009.

AlDosari, S.M., Banawas, S., Ghafour, H.S., Tlili, I. and Le, Q.H. (2023), "Drug release using nanoparticles in the cancer cells on 2-D materials in order to target drug delivery: A numerical simulation via molecular dynamics method", *Eng. Anal. Bound. Elem*., **148**, 34-40. https://doi.org/10.1016/J.ENGANABOUND.2022.12.020.

Aljaloud, A.S.M., Manai, L. and Tlili, I. (2023), "Bioconvection flow of cross nanofluid due to cylinder with activation energy and second order slip features", *Case Stud. Therm. Eng*., **42**, 102767, https://doi.org/10.1016/J.CSITE.2023.102767.

Babar, H. and Ali, H. M. (2019), "Towards hybrid nanofluids: preparation, thermophysical properties, applications, and challenges", *J Mol Liq*., **281**, 598-633. https://doi.org/10.1016/j.molliq.2019.02.102.

Banawas, S., Ibrahim, T.K., Tlili, I. and Le, Q.H. (2023), "Reinforced calcium phosphate cements with zinc by changes in initial properties: A molecular dynamics simulation", *Eng. Anal. Bound. Elem*., **147**, 11-21, https://doi.org/10.1016/J.ENGANABOUND.2022.11.033.

Bayones, F.S., Abd-Alla, A.M. and Thabet, E.N. (2022), "Magnetized dissipative soret effect on nonlinear radiative maxwell nanofluid flow with porosity, chemical reaction and joule heating", *Waves Random Complex Med*., 1-19. https://doi.org/10.1080/17455030.2021.2019352.

Benmansour, D.L., Kaci, A., Bousahla, A.A., Heireche, H., Tounsi, A., Alwabli, A.S., Alhebshi, A.M., Al-ghmady, K. and Mahmoud, S.R. (2019), "The Nano Scale Bending and Dynamic Properties of Isolated Protein Microtubules Based on Modified Strain Gradient Theory", *Adv. nano Res*, **7**(6), 443-457. https://doi.org/10.12989/ANR.2019.7.6.443.

Bhatti, M.M. and Abdelsalam, S.I. (2021), "Bio-inspired peristaltic propulsion of hybrid nanofluid flow with tantalum (Ta) and Gold (Au) nanoparticles under magnetic effects", *Waves Random Complex Med*., 1-26. https://doi.org/10.1080/17455030.2021.1998728.

Deville, M.O. (1990), "Chebyshev collocation solutions of flow problems", *Comput Methods Appl. Mech. Eng*., **80**(1-3), 27-37. https://doi.org/10.1016/0045-7825(90)90012-B.

El-gendi, S.E. (1969), "Chebyshev solution of differential, integral and integro-differential equations" , *Comput J*., **12**(3), 282-87. https://doi.org/10.1093/comjnl/12.3.282.

Ellahi, R., Wang, X. and Hameed, M. (2014), "Effects of heat transfer and nonlinear slip on the steady flow of couette fluid by means of chebyshev spectral method", *Zeitschrift für Naturforschung A*, **69**(1-2), 1-8. https://doi.org/10.5560/zna.2013-0060.

Farhana, K., Kadirgama, K., Rahman, M.M., Noor, M.M., Ramasamy, D., Samykano, M., Najafi, G., Sidik, N.A.C. and Tarlochan, F. (2019), "Significance of alumina in nanofluid technology", *J. Therm. Anal. Calorim*., **138**(2), 1107-1126. https://doi.org/10.1007/s10973-019-08305-6.

Henda, M. Ben, Alkanhal, T.A., Rebey, A., Musmar, S.A. and Tlili, I. (2023), "High-efficiency perovskite photovoltaic system performance by molecular dynamics method: Optimizing electron transport thicknesses, hole transport, and anti-reflector layers of the sustainable energy materials", *Eng. Anal. Bound. Elem*., **150**, 120-26, https://doi.org/10.1016/J.ENGANABOUND.2023.02.004.

Imtiaz, M., Shahid, F., Hayat, T. and Alsaedi, A. (2019). "Melting heat transfer in Cu-water and Ag-water nanofluids flow with homogeneous-heterogeneous reactions", *Appl. Math. Mech*., **40**(4), 465-80. https://doi.org/10.1007/s10483-019-2462-8.

Islam, N., Riasat, S., Ramzan, M.H., Ghazwani, A.S., Pasha, A.A., Kadry, S. and Eldin, S.M. (2023), "Thermal efficiency appraisal of hybrid nanocomposite flow over an inclined rotating disk exposed to solar radiation with arrhenius activation energy", *Alexandria Eng J*., **68**, 721-32. https://doi.org/10.1016/j.aej.2022.12.029.

Jiji, L.M. and Ganatos., P. (2010), "Microscale flow and heat transfer between rotating disks", *Int. J. Heat Fluid Flow*., **31**(4), 702-710. https://doi.org/10.1016/j.ijheatfluidflow.2010.02.008.

Khan, S.A., Hayat, T. and Alsaedi, A. (2022), "Simultaneous features of soret and dufour in entropy optimized flow of reiner-rivlin fluid considering thermal radiation", *Int. Commun. Heat Mass Transf*., **137**. https://doi.org/10.1016/j.icheatmasstransfer.2022.106297.

Khan, Z., Thabet, E.N., Abd-Alla, A.M. and Bayones, F.S. (2023), "Investigating the effect of bio-convection, chemical reaction, and motile microorganisms on prandtl hybrid nanofluid flow across a stretching sheet", *ZAMM J. Appl. Math. Mech*., e202300509, https://doi.org/10.1002/ZAMM.20230050.

Le, Q.H., Ali, Q., Al-Khaled, K., Amir, M., Riaz, S., Ullah Khan, S., Abdelmalek, Z. and Tlili, I. (2024), "Study of hybrid nanofluid containing graphene oxide and molybdenum disulfide nanoparticles with engine oil base fluid: A non-singular fractional approach", *Ain Shams Eng. J*., **15**(1), 102317, https://doi.org/10.1016/J.ASEJ.2023.102317.

Le, Q.H., Hussain, Z., Khan, N., Zuev, S., Javid, K., Khan, S.U., Abdelmalek, Z. and Tlili, I. (2023a), "Chebyshev collocation simulations for instability of hartmann flow due to porous medium: a neutral stability and growth rate assessment", *Ain Shams Eng. J*., **14**(12), 102215, https://doi.org/10.1016/J.ASEJ.2023.102215.

Le, Q.H., Smida, K., Abdelmalek, Z. and Tlili, I. (2023b), "Removal of heavy metals by polymers from wastewater in the industry: A molecular dynamics approach", *Eng. Anal. Bound. Elem*.,**155**, 1035-1342. https://doi.org/10.1016/J.ENGANABOUND.2023.07.0.

Letti, C.J., Costa, K.A.G., Gross, M.A., Paterno, L.G., Pereira-da-Silva, M.A., Morais, P.C. and Soler, M.A.G. (2017), "Synthesis, morphology and electrochemical applications of iron oxide based nanocomposites", *Adv. Nano Res*., **5**(3), 215-230. https://doi.org/10.12989/ANR.2017.5.3.215.

Li, C. and Tlili, I. (2023), "Novel study of perovskite materials and the use of biomaterials to further solar cell application in the built environment: A molecular dynamic study", *Eng. Anal. Bound. Elem*.,**155**, 425-31, https://doi.org/10.1016/J.ENGANABOUND.2023.06.018.

Lv, Y.P., Shaheen, N., Ramzan, M., Mursaleen, M., Nisar, K.S. and Malik, M.Y. (2021), "Chemical reaction and thermal radiation impact on a nanofluid flow in a rotating channel with hall current", *Sci Rep*., **11**(1). https://doi.org/10.1038/s41598-021-99214-y.

Mahanthesh, B., Gireesha, B.J., Animasaun, I.L., Muhammad, T. and Shashikumar, N.S. (2019), "MHD flow of SWCNT and MWCNT nanoliquids past a rotating stretchable disk with thermal and exponential space dependent heat source", *Phys. Scr*., **94**(8). https://doi.org/10.1088/1402-4896/ab18ba.

Parand, K., Mahdi Moayeri, M., Latifi, S. and Delkhosh, M. (2017), "A numerical investigation of the boundary layer flow of an eyring-powell fluid over a stretching sheet via rational Chebyshev functions", *Eur. Phys. J. Plus*., **132**(7). https://doi.org/10.1140/epjp/i2017-11600-0.

Patil, M.B., Shobha, K.C., Bhattacharyya, S. and Said, Z. (2023), "Soret and dufour effects in the flow of casson nanofluid in a vertical channel with thermal radiation: Entropy analysis", *J. Therm. Anal. Calorim.*, **148**(7), 2857-2867. https://doi.org/10.1007/s10973-023-11962-3.

Rashid, A., Dawar, A., Ayaz, M., Islam, S., Galal, A.M. and Gul, H. (2023), "Homotopic solution of the chemically reactive magnetohydrodynamic flow of a hybrid nanofluid over a rotating disk with brownian motion and thermophoresis effects", *ZAMM J. Appl. Math. Mech.*, **103**(8), e202200262. https://doi.org/10.1002/zamm.202200262.

Reddy, M.G., Naveen, K.R., Prasannakumara, B.C., Rudraswamy, N.G. and Kumar, K.G. (2021), "Magnetohydrodynamic flow and heat transfer of a hybrid nanofluid over a rotating disk by considering arrhenius energy", *Commun. Theor. Phys.*, **73**(4). https://doi.org/10.1088/1572-9494/abdaa5.

Reddy, Y.D. and Shankar Goud, B. (2023), "Comprehensive analysis of thermal radiation impact on an unsteady MHD nanofluid flow across an infinite vertical flat plate with ramped temperature with heat consumption", *Results Eng*., **17**. https://doi.org/10.1016/j.rineng.2022.100796

Renuka, A., Muthtamilselvan, M., Doh, D.H. and Cho, G.R. (2020), "Entropy analysis and nanofluid past a double stretchable spinning disk using homotopy analysis method", *Math. Comput. Simul*., **171**, 152-169. https://doi.org/10.1016/j.matcom.2019.05.008.

Rezaee, M., Yeganegi, A., Namvarpour, M. and Ghassemi, H. (2022), "Fluid flow dynamics in deformed carbon nanotubes with unaffected cross section", *Adv. Nano Res*., **12**(3), 253-261. https://doi.org/10.12989/ANR.2022.12.3.253.

Sharif, H., Khadimallah, M.A., Naeem, M.N., Hussain, M., Hussain, S. and Tounsi, A. (2021a), "Flow of MHD Powell-Eyring nanofluid: Heat absorption and Cattaneo-christov heat flux model", *Adv. Nano Res*., **10**(3), 221-234. https://doi.org/10.12989/ANR.2021.10.3.221.

Sharif, H., Khadimallah, M.A., Naeem, M.N., Hussain, M., Mahmoud, S.R., Al-Basyouni, K.S. and Tounsi, A. (2021b), "The investigation of magnetohydrodynamic nanofluid flow with arrhenius energy activation", *Adv. Nano Res*., **10**(5), 437-448. https://doi.org/10.12989/ANR.2021.10.5.437.

Shoaib, M., Raja, M.A.Z., Sabir, M.T., Awais, M., Islam, S., Shah, Z. and Kumam, P. (2021), "Numerical analysis of 3-D MHD hybrid nanofluid over a rotational disk in presence of thermal radiation with joule heating and viscous dissipation effects using Lobatto IIIA technique", *Alexandria Eng J*., **60**(4), 3605-3619. https://doi.org/10.1016/j.aej.2021.02.015.

Tlili, I., Alkanhal, T.A., Rebey, A., Henda, M. Ben and Musmar, S.A. (2023). "Nanofluid bioconvective transport for non-newtonian material in bidirectional oscillating regime with nonlinear radiation and external heat source: Applications to storage and renewable energy", *J. Energy Storage*, **68**, 107839. https://doi.org/10.1016/J.EST.2023.107839.

Vanaki, S.M., Ganesan, P. and Mohammed, H.A. (2016), "Numerical study of convective heat transfer of nanofluids: A review", *Renew Sustain Energy Rev*., **54**, 1212-1239. https://doi.org/10.1016/j.rser.2015.10.042.

Vijay, N. and Sharma, K. (2023), "Magnetohydrodynamic hybrid nanofluid flow over a decelerating rotating disk with soret and dufour effects", *Multidiscipl. Model. Mater. Struct*., **19**(2), 253-276. https://doi.org/10.1108/MMMS-08-2022-0160.

Wang, H., Zandi, Y., Gholizadeh, M. and Issakhov, A. (2021), "Buckling of porosity-dependent bi-directional fg nanotube using numerical method", *Adv. Nano Res*, **10**(5), 493-507. https://doi.org/10.12989/ANR.2021.10.5.493.

Yanzhen, Q., Zandi, Y., Rahimi, A., Pourkhorshidi, S., Roco-Videla, A., Khadimallah, M.A., Jameel, M., Kasehchi, E. and Assilzadeh, H. (2021), "Nano-SiO2 for efficiency of geotechnical properties of fine soils in mining and civil engineering", *Adv. Nano Res*, **11**(3), 301-12. https://doi.org/10.12989/ANR.2021.11.3.301.

Yasinskiy, A., Navas, J., Aguilar, T., Alcántara, R., Gallardo, J.J., Sánchez-Coronilla, A., Martín, E.I., De Los Santos, D. and Fernández-Lorenzo, C. (2018), "Dramatically enhanced thermal

properties for tio2-based nanofluids for being used as heat transfer fluids in concentrating solar power plants", *Renew Energy*., **119**, 809-19. https://doi.org/10.1016/j.renene.2017.10.057.

AT

Nomenclature

$r,\ \Phi,\ z$	Cylindrical coordinates system
$u,\ v,\ w$	Velocity components
$T,\ T_m,\ T_\infty$	Fluid, melting surface, ambient temperature, respectively
$C,\ C_m,\ C_\infty$	Fluid, melting surface, ambient concentration, respectively
$k^*,\ k_1,\ K$	Rosseland mean absorption, permeability, and effective thermal conductivity
$F=\frac{C_b}{rk_1^{\frac{1}{2}}},\ C_b$	Coefficient of the porous medium and drag force, respectively
$Q,\ D,\ B_0, (\rho C_p)$	Heat generation/absorption coefficient, mass diffusivity, strength of magnetic field, and heat capacitance
$C_p,\ Cs_1,\ Cs_2$	Specific heat at constant pressure, concentration susceptibility, and heat capacity of the solid surface
$F_r,\ M_1,\ Me,\ Rd$	Inertia, magnetic, melting, and radiation parameters, respectively
$Br,\ Pr,\ Re,\ Ec$	Brinkman, Prandtl, local Reynolds and Eckert numbers, respectively
$Du,\ Sr,\ Sc$	Dufour, Soret, Schmidt numbers, respectively
$f'(\eta),\ f(\eta),\ g(\eta)$	Radial, axial, and tangential velocity, respectively
$\tau_{wt},\ \tau_{w\Phi},\ j_{wt},\ q_w$	Radial stress, transverse shear stress, mass flux, and heat flux, respectively

Greek Symbols

$\mu,\ \nu,\ \rho$	Dynamics and kinematic viscosity, respectively and fluid density
$\sigma,\ \sigma^*,\ \alpha$	Electric conductivity, Stefen-Boltzman constant, and thermal diffusivity
$\eta,\ \eta^*,\ \lambda_3$	Transformed coordinate, porosity parameter, latent heat fluid
$\beta,\ \Omega,\ \varphi_1,\ \varphi_2$	Heat generation absorption parameter, constant angular velocity, volume concentration
$\theta(\eta),\ \phi(\eta)$	Dimensionless temperature and nanoparticles concentration, respectively

Subscript

hnf, nf	Hybrid Nanofluid and Nanofluid, respectively
$s1, s2$	Solid particles
m, ∞	Melting heat & mass transfer, and ambient, resbectively